Journal of Marine Research, 45, 1–32, 1987

Journal of
MARINE RESEARCH

Volume 45, Number 1

On the dynamics of the California Current system

by Julian P. McCreary, Jr.,[1] Pijush K. Kundu[1] and Shenn-Yu Chao[2]

ABSTRACT

The dynamics of the California Current system are studied using two ocean models, one with a shelf and one without. Both models are viscid and linearized about a background density field $\rho_b(z)$. Solutions are forced by steady and annually periodic winds with and without curl, and by an idealization of the observed wind field off California.

Solutions forced by a steady, equatorward, curl-free wind τ^y all have an equatorward surface coastal jet and a poleward undercurrent. Due to the β-effect and horizontal mixing, the circulation is not necessarily confined within a Rossby radius of the coast. The strength and structure of the currents vary considerably with parameters, the currents being stronger and broader when the forcing includes remote winds to the south and when ρ_b has a near-surface pycnocline. If τ^y oscillates at the annual cycle the response is qualitatively quasi-steady, but it also involves a poleward, offshore and vertical propagation of waves, and the maximum coastal current leads τ^y by several weeks.

Solutions forced by a steady, positive wind curl τ^y_x develop a deep, broad, poleward surface current near the coast, consistent with Sverdrup theory. Interestingly, there is also an equatorward surface flow located farther offshore, which exists because of the vertical mixing in the model. Solutions are not very dependent on model parameters, because they are primarily interior currents directly in balance with the wind curl and do not require the coast for their existence. If τ^y_x oscillates at the annual cycle, the response is not at all quasi-steady, and the maximum coastal current lags τ^y_x by 1–2 months.

Solutions forced by an idealization of the observed wind field off California compare favorably with observations, but only if ρ_b has a realistic pycnocline and the forcing includes remote winds off Baja California. Forcing by positive τ^y_x accounts for both the poleward Davidson Current during the winter and the equatorward flow located more than 100 km

1. Nova University Oceanographic Center, 8000 North Ocean Drive, Dania, Florida, 33004, U.S.A.
2. Horn Point Environmental Laboratories, University of Maryland, Cambridge, Maryland, 21613, U.S.A.

offshore throughout the year. The coastal jet forced by τ^y provides summertime equatorward flow within 100 km of the coast that is strong enough to reverse the poleward flow driven by τ^y_x.

1. Introduction

The prevailing winds off California, as along most other subtropical eastern ocean boundaries, are directed equatorward throughout the year. Such winds drive an offshore surface drift and force upwelling at the coast. As a consequence, near-surface isopycnals slope upward, the surface dynamic-height field slopes downward toward the coast, there is a geostrophically balanced surface jet that flows in the direction of the wind, and there is a poleward undercurrent at depths of 100–300 m. During the summer, the currents off California are consistent with this description. During the winter, however, a poleward surface current appears near the coast. This wintertime current, flowing against the direction of the local wind, is known as the Davidson Current (Sverdrup *et al.*, 1942; Hickey, 1979; Chelton, 1984). Its average speed is of the order of 10 cm/s, its width is about 80 km, and it is bounded to the west by the southward-flowing California Current that extends 1000 km offshore (Figs. 1a and 1b).

What mechanisms drive the Davidson Current against the wind? One possibility is *remote forcing* by winds located equatorward of the observations. For example, the wind field off Baja California can affect the currents off the California coast via the poleward radiation of coastally trapped waves. Another possibility is a *relaxation* of the local winds. In response to an equatorward wind a near-surface, poleward pressure gradient sets up at the coast, and this pressure gradient can drive a transient, poleward current if the wind subsequently relaxes. Consistent with this idea, the Davidson Current does appear when the alongshore component of the wind weakens (Fig. 1b). A third possibility is forcing by *wind curl*. The wind field off California strengthens offshore for 200 km, resulting in a region of positive wind curl near the coast (Fig. 1b). According to Sverdrup theory, the steady component of this curl forces a poleward current. Based on solutions to a steady-state, barotropic model, Munk (1950) first suggested that the Davidson Current is driven by this mechanism. Sverdrup theory in itself, however, cannot be a complete explanation for the current, because the observed flow is neither barotropic nor steady; moreover, the current appears when the wind curl is weakest (Fig. 1b).

A poleward coastal current may also be generated by *thermohaline forcing*. A poleward increase of the near-surface density field causes the sea surface to drop toward the pole. As a result, a geostrophic onshore current is generated in the ocean interior which bends poleward at an eastern ocean boundary. McCreary *et al.* (1986) have recently modelled this mechanism, and argued that it significantly drives the Leeuwin Current off the west coast of Australia. Wintertime sea-surface topography near California (Fig. 2b of Hickey, 1979), however, is not at all similar to that off Australia (Fig. 5 of Godfrey and Ridgway, 1985), with contours of surface dynamic

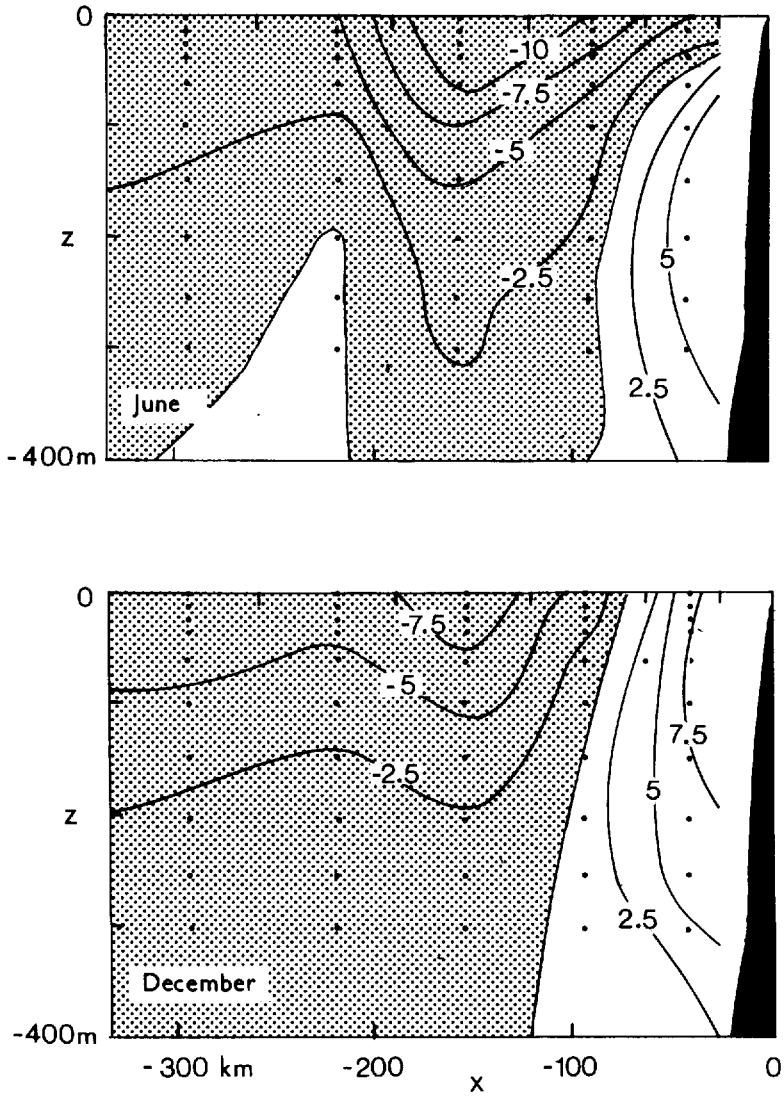

Figure 1a. Vertical sections of alongshore geostrophic velocity relative to 500 db along CalCOFI line 80 off Point Conception near 35N. Regions of equatorward flow are shaded. The Davidson Current appears during the winter, and there is equatorward flow centered about 150 km offshore throughout the year. (After Chelton, 1984.)

height off California bending equatorward rather than poleward. If thermohaline forcing is active off California, it seems to be overwhelmed by wind forcing.

As this research progressed it became apparent that an equally, if not more, important question than that posed above is: What mechanisms force equatorward flow off the California coast in a region of positive wind curl? Note in Figure 1a the

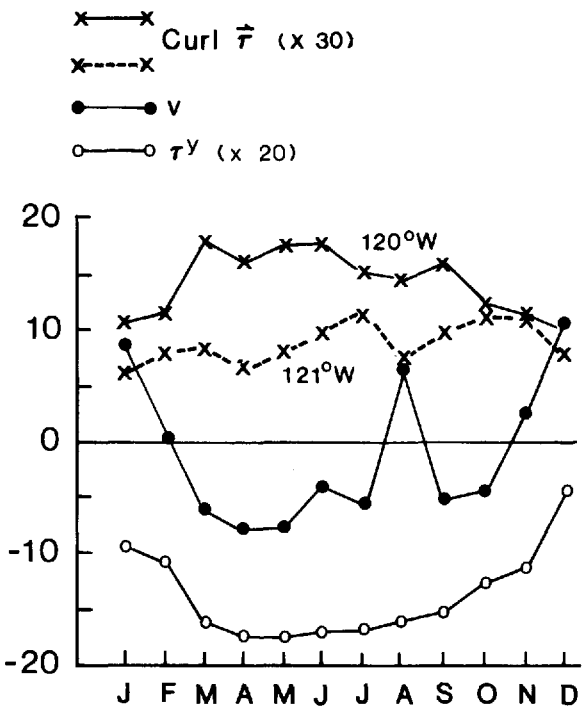

Figure 1b. The seasonal variation of alongshore geostrophic velocity, alongshore wind stress and wind curl off Point Conception near 35N. Their units are cm/s, dyn/cm^2 and dyn/cm^2/100 km, respectively. The variation of wind curl is shown at two positions, near the coast and 100 km offshore. The Davidson Current appears when both wind stress and wind curl are weakest. (After Hickey, 1979).

southward current centered about 150 km offshore that appears to intensify and extend shoreward during the summer. To our knowledge, as yet no mechanism has been proposed to account for this current. One possible mechanism for driving this equatorward flow is the *alongshore wind* which generates a coastal jet, but that jet is typically trapped closer to the coast than 150 km. An important result of this study is that another source is the *positive wind curl* itself. [There is a weak, negative wind curl offshore of 200 km (Hickey, 1979; her Figs. 4 and 17), which can drive an equatorward drift in the Pacific interior. However, it is unlikely that this forcing can account for the strong equatorward current located only 150 km offshore.]

The purpose of this paper is to investigate the dynamics of the California Current system. In particular, the study is focussed around providing answers to the two questions posed above, namely, (1) what drives the Davidson Current against the wind, and (2) what generates the equatorward flow in a region of positive wind curl. Many of our results, however, are not closely tied to the situation off California, and have a general applicability. Two different linear, viscid, continuously stratified models are

used. One is the analytic, flat-bottom model of McCreary and Kundu (1985), and the other is a modified version of the numerical shelf model of McCreary and Chao (1985), generalized to allow for the periodic forcing. Solutions are forced by steady and periodic winds with and without curl, are contrasted for various choices of model parameters, and their dynamics are discussed.

Solutions are also forced by an idealized representation of the observed wind field off California. One of them, employing a realistic background pycnocline and including remote winds off Baja California, compares favorably with observations. Some conclusions concerning the California Current system are the following. Positive wind curl drives both the Davidson Current and the equatorward flow located more than 100 km offshore. The alongshore wind forces a coastal jet that is broadened by the pycnocline and the β-effect, and strengthened by the remote winds. During the summer this jet is strong enough to reverse the poleward current driven by wind curl.

2. The ocean models

The two ocean models used are very similar to those discussed extensively in McCreary and Kundu (1985) and McCreary and Chao (1985). For this reason only a brief description of the equations of motion and boundary conditions is provided here. Readers interested in mathematical details should consult the earlier papers.

a. The flat-bottom model

The equations of motion for both models are linearized about a stably stratified background density state $\rho_b(z)$ with associated Väisälä frequency $N_b(z)$, and they are forced by a meridional wind stress of the form $\tau^y(x, y)e^{-i\sigma t}$. The complex amplitudes of the flow variables satisfy

$$\begin{aligned} -fv + p_x &= 0, \\ -i\sigma v + fu + p_y &= G + (\nu v_z)_z + \nu_h v_{xx}, \\ -i\sigma\rho - \frac{N_b^2}{g} w &= (\kappa\rho_z)_z + \kappa_h\rho_{xx}, \\ p_z &= -\rho g, \\ u_x + v_y + w_z &= 0, \end{aligned} \tag{1}$$

where all symbols have their usual meaning. The Coriolis parameter is $f = 2\Omega\sin(y/R)$, where $\Omega = 2\pi/\text{day}$ and R is the radius of the earth. For convenience, we adopt unit Prandtl numbers so that $\nu = \kappa$ and $\nu_h = \kappa_h$. A meridional wind stress enters the ocean as a body force $G(x, y, z) = \tau^y(x, y)\, Z(z)$, where $Z(z)$ is any function such that its integral over the water column is unity. The restriction on $Z(z)$ ensures that the vertical integral of G yields the wind stress τ^y at the sea surface.

These equations involve two key assumptions: the alongshore flow is taken to be

geostrophic, and the Laplacian operator in the horizontal mixing terms is replaced by ∂_{xx}. Physically, the effect of these restrictions is to filter out of the system all waves with equatorward group velocity or with equatorward decay. Mathematically, their effect is to ensure that only first-order y-derivatives are involved in the solution of equations (1), so that the system is essentially parabolic in y. As a result, solutions can be determined by means of a poleward integration.

When N_b is a function of z, two additional assumptions are: the vertical mixing of heat is replaced by $(\kappa\rho)_{zz}$, and the vertical mixing coefficients are inversely proportional to N_b^2. These restrictions are necessary in order to be able to represent solutions simply as expansions in uncoupled vertical modes $\psi_n(z)$. Boundary conditions are

$$\begin{aligned} &w = \kappa\rho = \nu v_z = 0, && \text{at } z = 0, -H, \\ &u = v = 0, && \text{at } x = 0, \\ &\text{solution is bounded} && \text{as } x \longrightarrow -\infty, \end{aligned} \tag{2}$$

where H is the water depth. The assumption of zero stress at the ocean surface is sensible since wind stress is introduced entirely through the body force $G(x, y, z)$. The surface and bottom values of $\kappa\rho$ and bottom stress are fixed to be zero to ensure that solutions can be represented as vertical-mode expansions.

It is worth noting that the boundary conditions on ρ are not independent from the others. Because of the assumption of alongshore geostrophy, the thermal wind relation $v_z = -g\rho_x/f$ holds everywhere. The zero-stress conditions at the surface and bottom then ensure that $\rho_x = 0$ there, and $\rho = 0$ follows from the boundedness of the far field and the lack of thermal forcing.

b. The shelf model

Equations of motion for the shelf model are again (1). They can be combined into a fourth-order equation in p alone, which can then be separated into the two coupled, second-order equations

$$\begin{aligned} \phi &= \nu p_{zz} + \nu_h p_{xx} + i\sigma p, \\ f^2\left(\frac{\phi_z}{N_b^2}\right)_z + \phi_{xx} &= \beta p_x. \end{aligned} \tag{3}$$

The velocity and density fields are easily expressed in terms of p and ϕ.

Boundary conditions are

$$\begin{aligned} &w = \nu v_z = 0, && \text{at } z = 0, \\ &w = -uh_x, \nu v_z = \gamma v, && \text{at } z = -h(x), \\ &u = v = 0, && \text{at } x = 0, \\ &p_{xx} = \phi_{xx} = 0, && \text{at } x = -L, \end{aligned} \tag{4}$$

where $h(x)$ is the variable depth of the ocean, and the numerical grid extends offshore to an artificial open boundary at $x = -L$. In contrast to the flat-bottom model, ν is assumed depth-independent here. Bottom drag with coefficient γ is imposed on the bottom boundary. The presence of a shelf, the bottom condition on ν, and the vertical distribution of ν are the only dynamical differences between the shelf and flat-bottom models.

The present model differs from that of McCreary and Chao (1985) in the inclusion of the periodic term $i\sigma p$ in (3), and the use of no-slip conditions at $x = 0$ and "slip" conditions at $x = -L$ in (4). The numerical scheme differs in that Eqs. (3) are solved at boundary, as well as at interior grid points. As a result, all boundary conditions are imposed using center-differenced, rather than single-sided, derivatives. An extra set of grid points located beneath the bottom is required to impose the bottom conditions.

3. Results for the flat-bottom model

The solutions in sections 3a and 3b are forced by a wind field with the separable form

$$\tau^y = \tau_o X(x) Y(y) e^{-i\sigma t}, \tag{5}$$

and the forcing is either purely steady ($\sigma = 0$) or oscillatory at the annual period ($\sigma = 2\pi$/year). The wind strength τ_o is -1 dyn/cm^2 for steady forcing so that the wind is directed equatorwards, and is 1 dyn/cm^2 for periodic forcing. The wind field forcing the solutions in section 3c is a linear combination of wind fields having the form (5), and is defined in that section.

For calculations without wind curl, the zonal distribution is $X(x) = 1$. For calculations with wind curl, it is

$$X(x) = \begin{cases} \sin \dfrac{\pi |x|}{2\Delta}, & -\Delta < x \le 0 \\ 1, & x \le -\Delta, \end{cases} \tag{6}$$

where $\Delta = 200$ km. This profile, indicated in Figure 5, is similar to the observed structure of the wind field off California (Nelson, 1977; Hickey, 1979; Chelton, 1984). With $\tau_o = -1$ dyn/cm^2 there is a maximum positive curl at the coast of 0.78 dyn/cm^2 per 100 km. According to (6), $X(x)$ and hence τ^y vanish at the coast; this choice was made in order to isolate the response forced by wind curl τ^y_x from that forced by the coastal value of τ^y.

The latitudinal distribution of the stress is

$$Y(y) = \begin{cases} \frac{1}{2}[1 + \cos \pi(y - y_o - 2.5°)/2.5°], & y_o \le y < y_o + 2.5° \\ 1, & y_o + 2.5° \le y < 37.5° \\ \frac{1}{2}[1 + \cos \pi(y - 37.5°)/2.5°], & 37.5° \le y \le 40° \\ 0, & \text{otherwise,} \end{cases} \tag{7}$$

where y_o is either 20N or 30N. This structure with y_o = 20N is indicated in Figure 4.

The vertical profile of the body force is

$$Z(z) = \frac{2}{d}\left(\frac{\ln 10}{\pi}\right)^{1/2} e^{-(\ln 10)z^2/d^2}. \tag{8}$$

It decays in depth with a ten-folding scale of d = 60 m, and satisfies the integral constraint $\int_{-H}^{0} Z(z)dz = 1$.

Two background density fields are adopted. One is the linear profile

$$\rho_b = 1 - \Delta\rho\left(\frac{z}{H}\right), \tag{9}$$

where $\Delta\rho$ = 0.004 gm/cm^3 and H = 1000 m, giving $N_b = 0.63 \times 10^{-2}$ s^{-1}. The other is

$$\rho_b = \begin{cases} 1, & z \ge -h \\ 1 + \Delta\rho_1[1 - e^{-(z+h)/b_1}] + \Delta\rho_2[1 - e^{-(z+h)/b_2}], & -H \le z < -h, \end{cases} \tag{10}$$

with h = 25 m, $\Delta\rho_1$ = .0015 gm/cm^3, b_1 = 75 m, $\Delta\rho_2$ = .001 gm/cm^3 and b_2 = 500 m. This profile has a strong near-surface pycnocline similar to the observed one off California (Lynn *et al.*, 1982; Reid, priv. comm.; Chelton, priv. comm.).

The depth of the ocean is H = 1000 m for all of the solutions shown in the figures. This shallow depth was used in order to be able to compare closely the flat-bottom and shelf solutions. Solutions, however, are not very sensitive to this parameter.

The values of the mixing parameters are usually $\nu_h = 10^6$ cm^2/s and ν = 10 cm^2/s, but in a few cases they are 10^5 and 1 cm^2/s, respectively. For the background density field (10), ν varies with depth, in which case its value is given at a depth of 75 m.

Solutions have been found for each of the wind fields described above and for many different combinations of model parameters. For convenience, Table 1 summarizes the parameter values used for the various solutions reported here. There are several references in this section to parts of section 5, which provide dynamical explanations for many of the interesting features of solutions.

Table 1. Model parameters used for the solutions discussed in this paper. The background density profiles $\rho_b(z)$ either are linear or have a pycnocline, and they are defined in (9), (10) and (13). The vertical mixing coefficient ν varies with depth for the flat-bottom solutions when $\rho_b(z)$ has a pycnocline, and in that case the table gives its value at a depth of 75 m. If the bottom topographic profile $h(x)$ is flat, the table gives the ocean depth H; otherwise the shelf profile is defined in (12). Units for the mixing parameters are cm^2/s and for H are meters.

Case	ν_h	$\rho_b(z)$	y_o	ν	$h(x)$
a	10^5	linear	30N	10	1000
b	10^6	linear	30N	10	1000
c	10^6	pycnocline	30N	10	1000
d	10^6	pycnocline	20N	10	1000
e	10^6	pycnocline	20N	1	1000
f	10^6	pycnocline	20N	10	2500
g	10^6	pycnocline	20N	10	shelf

a. Solutions forced by τ^y

As noted in the Introduction, it became clear to us during the course of this research that, if the model was ever going to produce a reasonable simulation of the California Current system, it would have to be able to generate significant equatorward flow off the California coast. The solutions in Figure 2 are organized to illustrate the parameter choices that are required to generate such a flow within 100 km of the coast. The figure contrasts solutions that are forced by a steady equatorward wind without curl, the four panels showing v for Cases a–d of Table 1 on zonal sections at 35N. The structures of all four solutions are similar, each having an equatorward surface jet and a poleward undercurrent, but they differ considerably in their strength and offshore extent. In Case a, the alongshore current is sizeable, but it is narrowly confined to the coast. In Case b, ν_h is increased to 10^6 cm^2/s, and as expected the circulation spreads offshore and weakens. In Case c, the linear density profile (9) is replaced by the more realistic profile (10), and the surface current extends twice as far offshore as it does in Case b (see section 5c). Finally, in Case d remote winds to the south are included in the forcing by changing y_o to 20N, and the strength of the surface current is more than double that in Case c (see section 5c). Thus, whether there is a significant, broad equatorward flow depends very much on both the presence of a strong near-surface pycnocline and of remote winds.

Figure 3 contrasts solutions for Cases a and d when the wind oscillates at the annual cycle, the left and right panels showing the amplitude and phase of v on zonal sections at 35N. Positive phase indicates that v leads the wind. Both solutions exhibit a quasi-steady character in that the structures of v are very similar to those of the corresponding steady solutions in Figure 2 (see section 5c). At $t = 6$ months, for example, when the wind is most equatorward, the currents are poleward in regions where the phase is unshaded and equatorward in shaded regions, and at that time

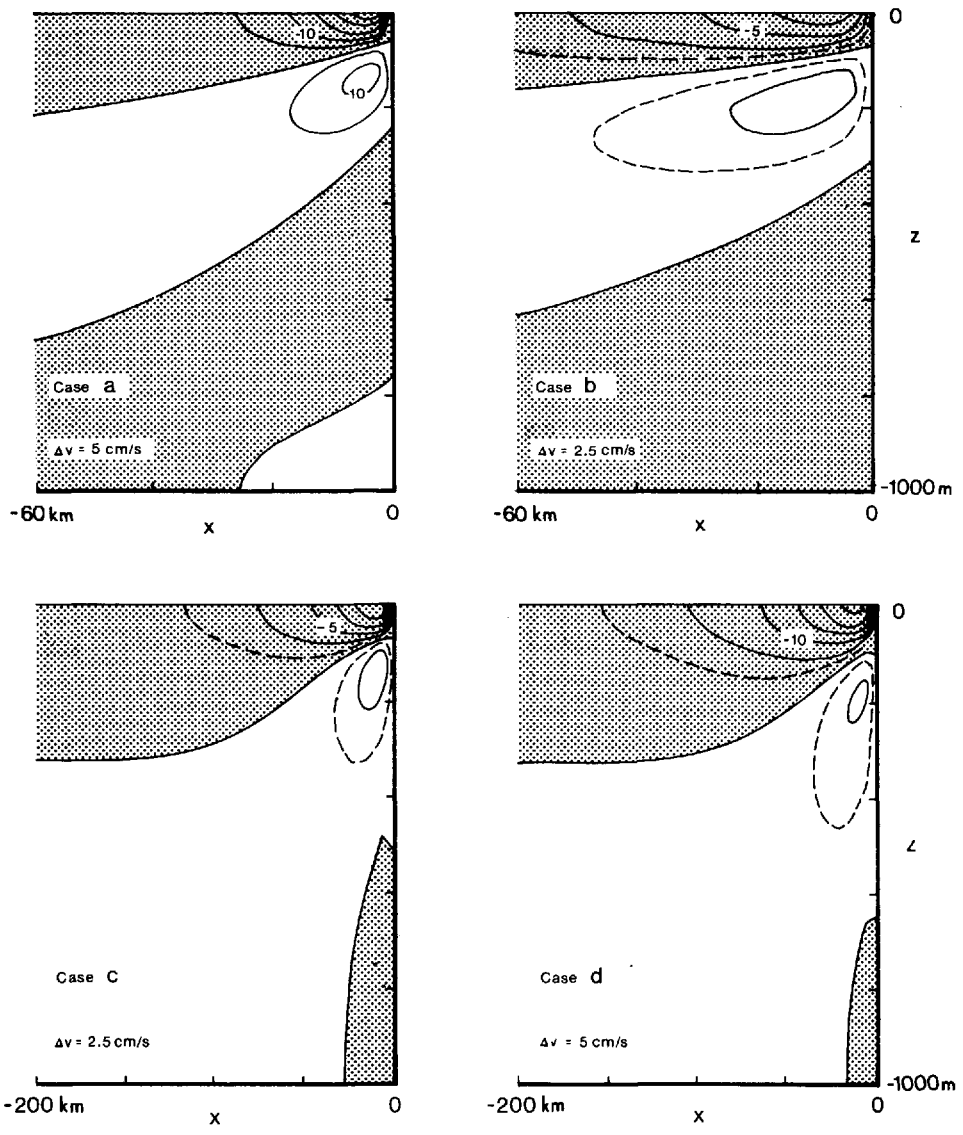

Figure 2. Zonal sections at 35N contrasting ν for Cases a-d in Table 1 when the wind is steady and without curl. Dashed contours are $\pm\Delta\nu/2$, and regions of negative (equatorward) flow are shaded. Note that the offshore extent of the sections differs between the upper and lower panels. The solutions illustrate how horizontal mixing, background density field and remote forcing affect the response. A strong, near-surface pycnocline and remote forcing are both necessary in order to generate a significant equatorward current offshore.

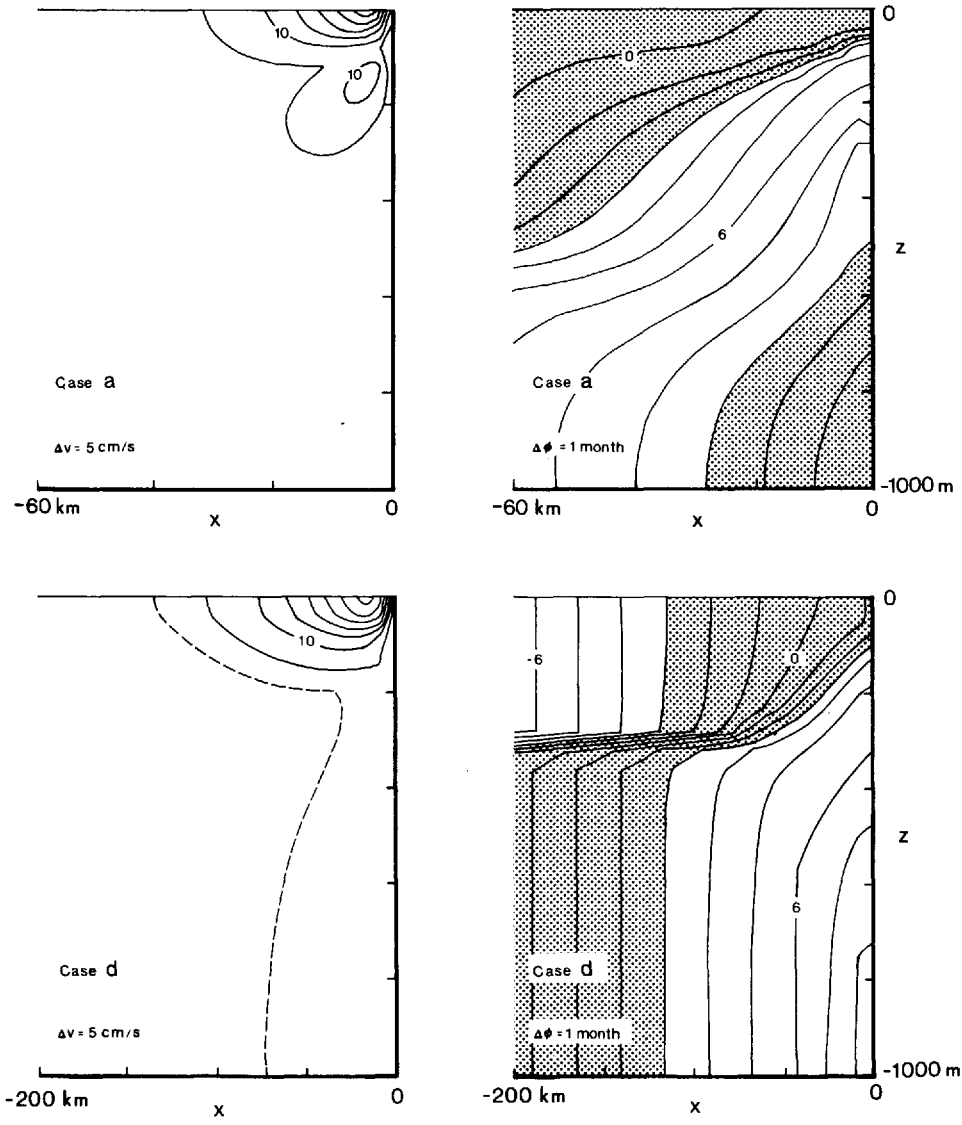

Figure 3. Zonal sections at 35N contrasting v for Cases a and d in Table 1 when the wind is annually periodic and without curl. The figure shows the amplitude and phase of v in the left and right panels, respectively. The dashed contour is 2.5 cm/s. Positive phase indicates that v leads the wind. Regions where the phase lead is less than 3 months or greater than 9 months are shaded; thus, at $t = 6$ months when the wind is directed equatorward, the currents are equatorward (poleward) in the shaded (unshaded) regions. Both solutions appear quasi-steady, being similar in amplitude and structure to their steady counterparts in Figure 2. For Case a there is an indication of the offshore propagation of the $n = 1$ Rossby wave. For Case d the offshore propagation of phase is associated with the $n = 1$, β-plane Kelvin wave. In both cases the maximum surface current leads the wind by several weeks.

corresponding solutions have very nearly the same amplitude and structure. Another indication of quasi-steadiness is that near the coast phase changes rapidly across a relative minimum in amplitude. On the other hand, the solutions also have properties that are not quasi-steady. In both cases there is upward and offshore propagation of phase, with the maximum surface current leading the wind by a few weeks (see section 5c). In Case a, offshore phase changes relatively rapidly near a depth of 500 m, indicating the offshore propagation of an $n = 1$ Rossby wave; in Case d, there is a similar rapid change of phase near 300 m, due to the offshore propagation associated with the $n = 1$, β-plane Kelvin wave (see section 5c).

Figure 4 shows v for Case d on an alongshore section at $x = -15$ km, the offshore distance near which the surface current reaches its maximum speed. The current increases in strength to 40N, the northern limit of the wind field, and extends well beyond that point (see section 5c). Physically, the reason for this increase is that at $t = 0$ there is Ekman drift into the coast throughout the forcing region, and the coastal current must strengthen poleward in order to provide a northern exit for this inflow (see section 5c). Phase lines slope downward toward the pole, indicating that part of the coastal signal is a vertically propagating, β-plane Kelvin wave carrying energy poleward and downward along the boundary (see section 5c).

One implication of the above solutions is that remote forcing by curl-free winds cannot account for the appearance of the Davidson Current. Although in all the solutions the surface currents are strongly influenced by remote winds, they always flow in the same direction as the wind (except for the periodic solution for a brief period of time when the wind changes direction). Since the wind field off Baja California (and that located even farther to the south) is directed equatorward throughout the year, it cannot remotely force a poleward current along the California coast.

Another implication is that the low-frequency relaxation of the wind associated with the annual cycle cannot generate the Davidson Current. An idealized version of the alongshore wind at the California coast is $\tau^y = \tau_o\, Y(y)\, (.5 + .4e^{-i\sigma t})$ with $\tau_o = -1$ dyn/cm^2, as in (11) below. Solutions forced by this wind are an appropriate combination of the steady and periodic solutions discussed above. Because the amplitudes of the periodic solutions are somewhat larger than those of their steady counterparts, a poleward surface current can occur near the time $t = \pi/\sigma$ even though the wind never reverses direction. However, the resulting poleward flow does not much resemble the Davidson Current, being too shallow and too weak. [Whether a sizeable poleward current results from a wind relaxation does depend on how rapidly the relaxation occurs. For example, a large current is produced if the wind suddenly switches off (Philander and Delecluse, 1983). No such rapid relaxation, however, takes place off California as part of the annual cycle.]

It is noteworthy that the solutions in Figure 4 do not at all resemble a similar solution reported by Philander and Yoon (1982). These authors studied the response of the coastal ocean to a low-frequency ($\sigma = 2\pi/200$ day^{-1}) wind field without curl, using

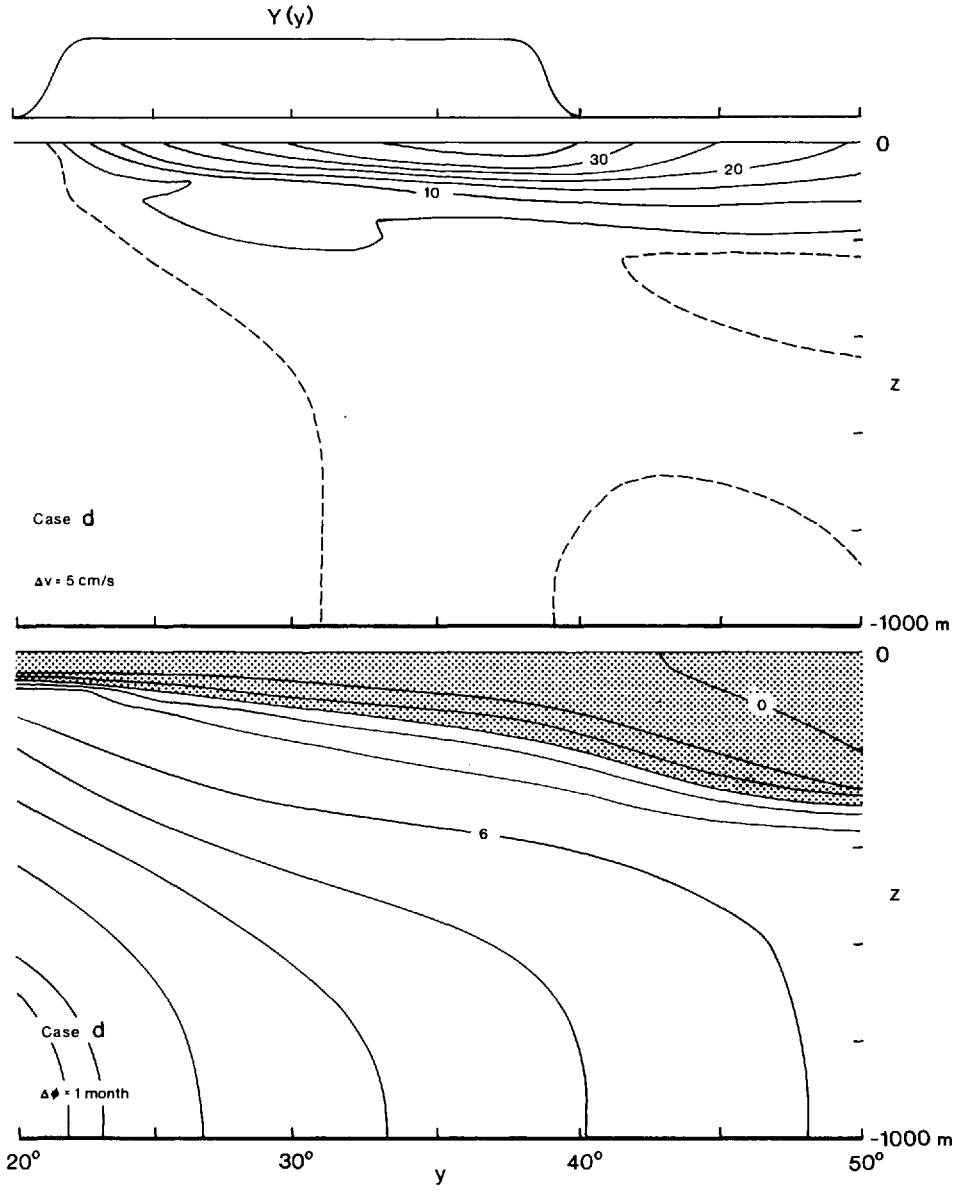

Figure 4. Meridional sections showing the amplitude and phase of v for Case d when the wind is annually periodic and without curl. Each section is located at $x = -15$ km, the distance offshore at which v attains its maximum value (Fig. 3). The dashed contour is 2.5 cm/s. Positive phase indicates that v leads the wind. The meridional structure of the wind is indicated at the top of the figure and is defined in (7). The flow increases steadily throughout the region of the wind, and extends well to the north. Phase lines slope down toward the north, indicating the presence of a vertically propagating, β-plane Kelvin wave.

a nonlinear, continuously stratified, flat-bottom general circulation model. In contrast to the solutions in Figure 4, their response did not appear to be at all quasi-steady, but rather was dominated by bands of alternating northward and southward surface currents associated with the offshore propagation of an $n = 1$ Rossby wave (see their Figs. 12 and 13). We performed a series of experiments with our flat-bottom model to investigate the reasons for this difference in response. One of our solutions, using a wind field and parameter values similar to theirs, compared remarkably well with their solution. We concluded that the difference in response was due to their use of strong horizontal mixing ($\nu_h = 10^7$ cm^2/s), which weakened and broadened the quasi-steady part of the response to such a degree that it was no longer apparent, and to the low-latitude location of their solution which considerably increased the zonal wavelength of the $n = 1$ Rossby wave.

b. Solutions forced only by τ_x^y

Figure 5 contrasts solutions for Cases a–d that are forced by a steady equatorward wind with the zonal structure (6), so that the wind vanishes at the coast but wind curl does not. In contrast to the flows driven by τ^y (Fig. 2), the four solutions are similar in both structure and magnitude. The reason for this similarity is that much of the flow in each solution is directly in balance with the interior wind curl, and does not require the coast for its existence (see section 5b). The surface currents extend deeper into the water column than those driven by τ^y (Fig. 2), and there is no undercurrent. In Cases c and d the introduction of the pycnocline traps the current closer to the surface as expected. A comparison of Cases c and d shows that the addition of remote wind curl does not strengthen the current (unlike the addition of remote curl-free winds), but in fact weakens it somewhat (see also Fig. 6). An interesting feature in all the solutions is the presence of equatorward surface flow located more than 100 km offshore but still in a region where wind curl is positive. Sverdrup theory cannot account for this current; its existence is due entirely to the vertical diffusion in the model (see section 5b).

Figure 6 is an alongshore section of the solution in Figure 5 for Case d, located 15 km offshore. As noted in the preceding paragraph, much of this flow is an interior current that exists independent of the coast. Another part increases rapidly in strength from 20N–22.5N, weakens gradually to 37.5N, and reverses beyond 40N. This part exists only because there is a coast, and is driven by zonal, geostrophic interior currents confined near the northern and southern edges of the wind (see section 5c). Figure 6 explains why the current for Case c in Figure 5 is stronger than that for Case d: the Case c solution (with $y_o = 30$N) is located closer to the southern edge of the wind.

Figure 7 contrasts the solutions for Cases a and d when the wind-curl field oscillates at the annual cycle. Neither flow field is at all quasi-steady. The structures of both amplitudes differ considerably from their steady counterparts in Figure 5, phase lines near the coast do not change rapidly across a relative minimum in amplitude, and the maximum surface current near the coast lags the wind curl by 1–2 months. In Case a,

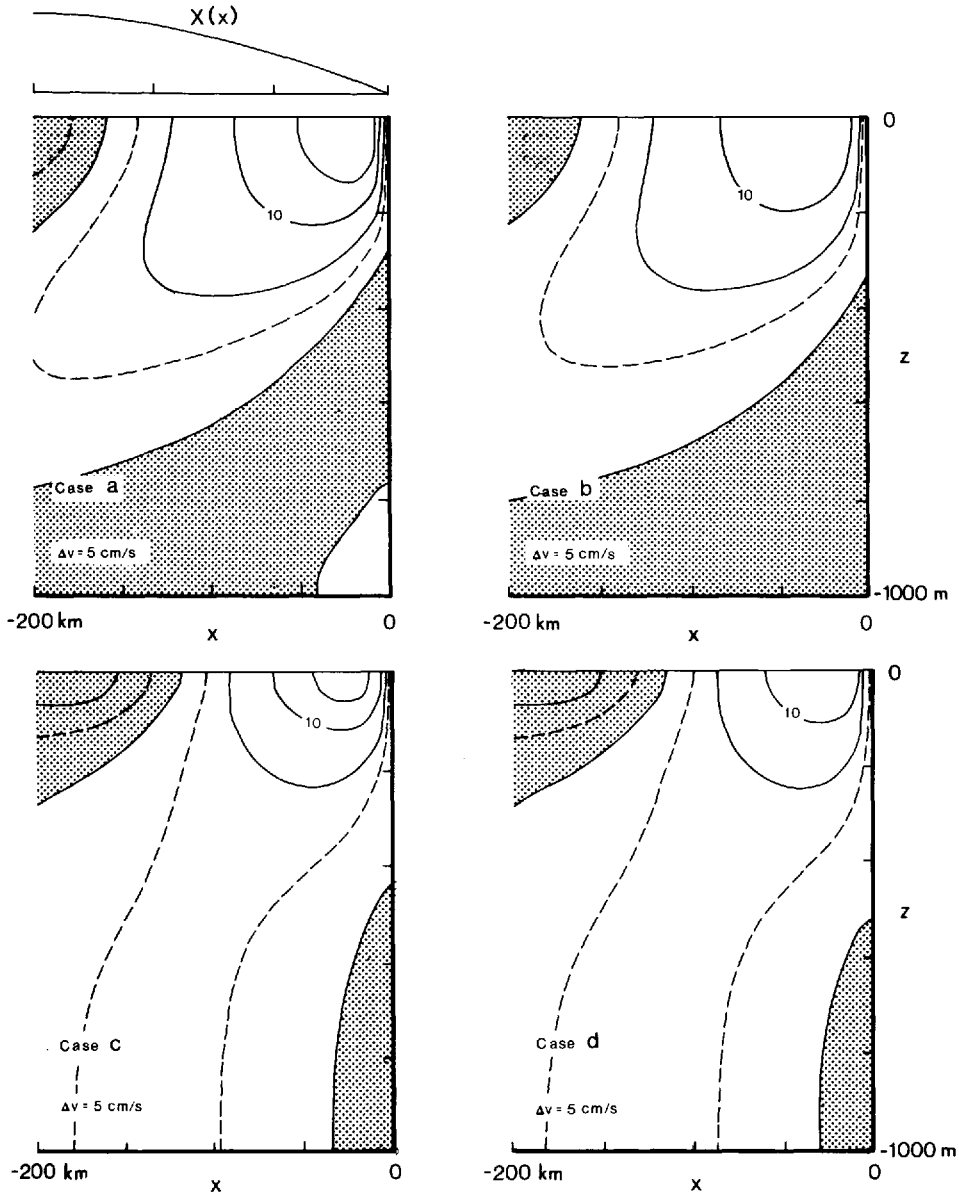

Figure 5. Zonal sections at 35N contrasting v for Cases a-d in Table 1 when there is a steady wind curl near the coast and $\tau^y = 0$ at $x = 0$. Dashed contours are ± 2.5 cm/s and regions of negative (equatorward) flow are shaded. The zonal structure of the wind is indicated at the top of the figure and is defined in (6). In contrast to the solutions forced by a wind without curl (Fig. 2), the surface current is directed poleward and extends more deeply into the water column, and there is no undercurrent. There is equatorward flow offshore even though the wind curl is positive there.

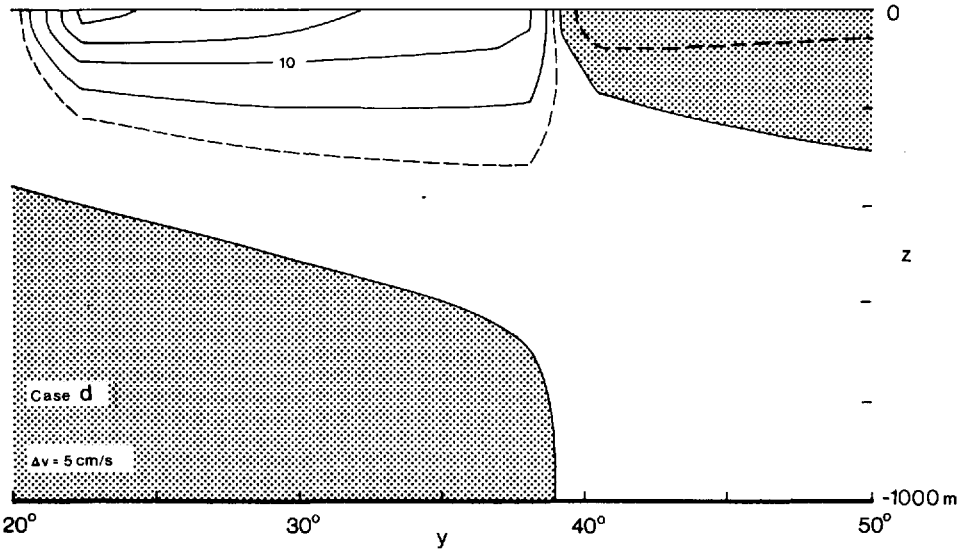

Figure 6. Meridional section showing v for Case d when there is a steady wind curl near the coast and $\tau^y = 0$ at $x = 0$. Dashed contours are ± 2.5 cm/s, and regions of negative (equatorward) flow are shaded. The section is located at $x = -15$ km. Part of the flow is an interior current directly in balance with the forcing. Another part is a coastal current forced by zonal geostrophic interior currents located near the northern and southern edges of the wind.

the solution shows a relative minimum in offshore amplitude at a depth of 500 m across which phase changes somewhat rapidly, indicating the offshore propagation of an $n = 1$ Rossby wave. In Case d there are two relative maxima in amplitude at the surface. The offshore maximum is an interior current that is directly in balance with the forcing (see section 5b). The nearshore maximum also includes a coastal contribution, predominantly an $n = 1$, β-plane Kelvin wave forced by zonal, geostrophic interior currents (see section 5c).

c. The California Current system

The observed wind field off California has a complicated spatial and temporal structure (Nelson, 1977; Hickey, 1979); however, it also has dominant characteristics that can be represented by simple functions. According to Figure 1b, the alongshore wind and its curl have nonzero means, and their annual components are approximately in phase, with their maximum and minimum strengths occurring roughly in June and December, respectively. Accordingly, an idealized representation of the wind field is taken to be

$$\tau^y = \tau_o Y(y)(.5 + .4e^{-i\sigma t}) + \tau_o X(x)\, Y(y)(.45 + .15e^{-i\sigma t}), \qquad (11)$$

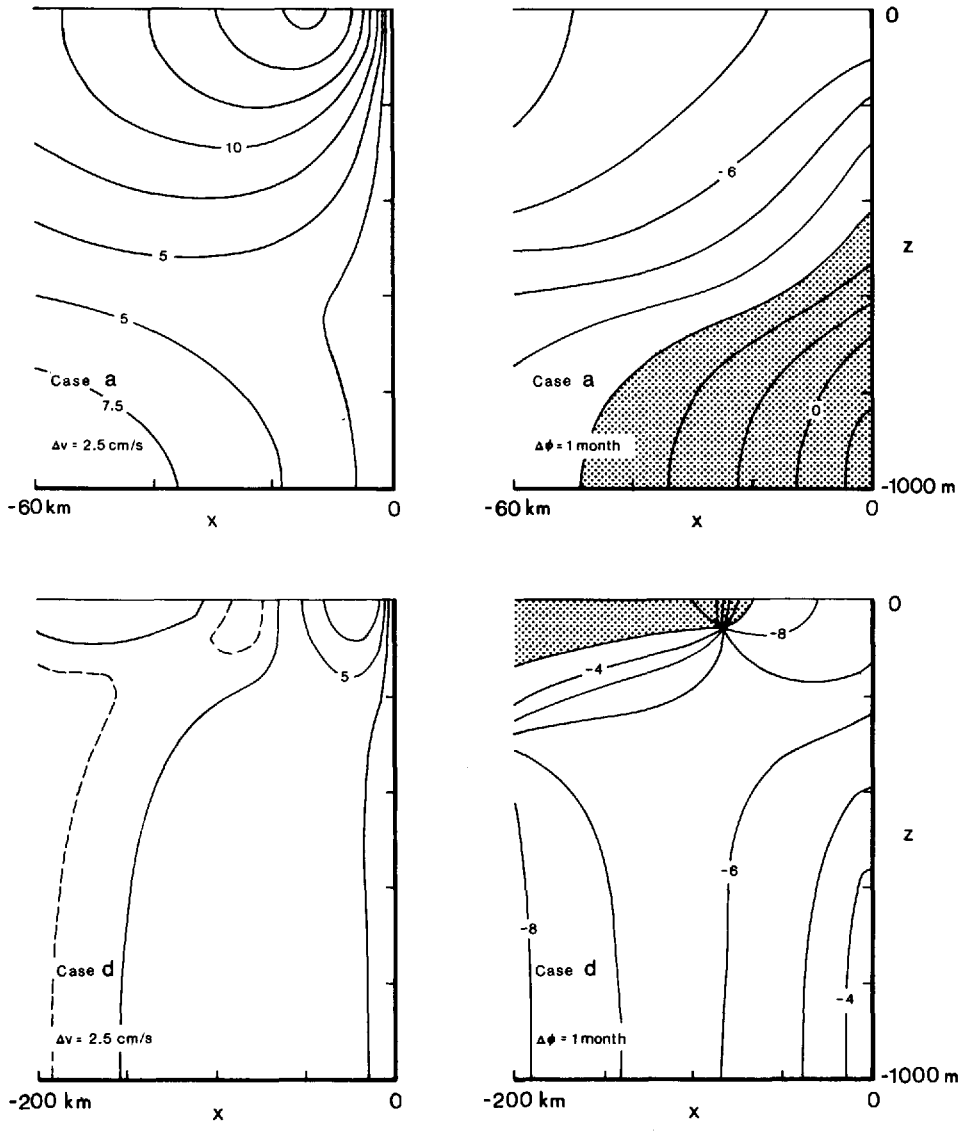

Figure 7. Zonal section at 35N contrasting v for Cases a and d in Table 1 when there is an annually periodic wind curl near the coast and $\tau^y = 0$ at $x = 0$. The figure shows the amplitude and phase of v in the left and right panels, respectively. Dashed contours are 1.25 cm/s. For Case a the offshore propagation of an $n = 1$ Rossby wave is apparent. For Case d the offshore relative maximum of $|v|$ is an interior current directly in balance with the wind forcing, whereas the nearshore maximum is a coastal current forced by zonal, geostrophic interior currents located near the northern and southern edges of the wind. In both cases the response is not at all quasi-steady, and the maximum surface current lags the wind curl by about 1–2 months.

where $t = 0$ corresponds to June, $\tau_o = -1$ dyn/cm^2, $\sigma = 2\pi$/year, and $X(x)$ and $Y(y)$ are given in (6) and (7), respectively. The response of the model to (11) is therefore an appropriate linear combination of the four types of solutions discussed above, and hence is easy to interpret dynamically.

The forcing (11) neglects the following features of the observed wind field: (1) the winds north of 40N, (2) the broad region of weak, negative curl offshore of 200 km, and (3) shifts in the amplitude and phase of the wind along the coast (Nelson, 1977; Hickey, 1979). The first two features have no effect on the model response in our region of interest ($x > -200$ km, $y < 40$N), since waves in the model carry information only poleward and westward. We purposely neglected the third feature to ensure that our solutions were easier to interpret.

Figure 8 shows the seasonal variation of ν for Case d on a zonal section at $y = 35$N at four times of the year. The sequence of panels illustrates a competition between the equatorward and poleward surface currents forced by τ^y and τ^y_x, respectively. In June, when τ^y dominates the forcing, there is a strong coastal jet and an undercurrent, and the surface current is everywhere equatorward. Note the similarity between the response in this season and that for Case d in Figure 2. By September, due to the weakening of τ^y, the coastal jet no longer appears as a distinct current. In December, τ^y_x dominates the forcing and there is a broad poleward surface current within 100 km of the coast, the model Davidson Current. Now the response looks quite like that for Case d in Figure 5. From December to March τ^y strengthens, the coastal jet intensifies and expands offshore, and the Davidson Current nearly vanishes.

Generally, the solution in Figure 8 compares favorably with observations. A limitation of the solution, however, is that the equatorward flow offshore of 100 km is too weak and somewhat too shallow. The reason for this failure is not clear. One possibility is that the vertical mixing in the model is not large enough (section 5b). Another possibility is that (6) is not a sufficiently accurate description of the zonal structure of the wind off California.

Figure 9 shows the solutions for Cases a and e at two times of the year. Both solutions do a poor job of simulating the California Current system. In Case a the surface current is poleward all year, except very near the coast in June. In addition, there is only a very weak seasonal cycle, with the maximum surface flow being only somewhat stronger in December (7.3 cm/s) than in June (6.3 cm/s). The reason for this failure is traceable to the fact that the equatorward coastal current forced by τ^y does not spread far enough offshore to be able to counteract the poleward flow forced by τ^y_x. In Case e the poleward flow forced by τ^y_x is too strong. The decrease in ν allows the response to steady τ^y_x to adjust closer to Sverdrup balance, resulting in a poleward current that is more surface trapped and considerably stronger. Consequently, during the summer the equatorward flow due to τ^y is not strong enough to reverse the poleward flow everywhere offshore.

To test the effect of bottom depth, we repeated the solution of Figure 8 with H

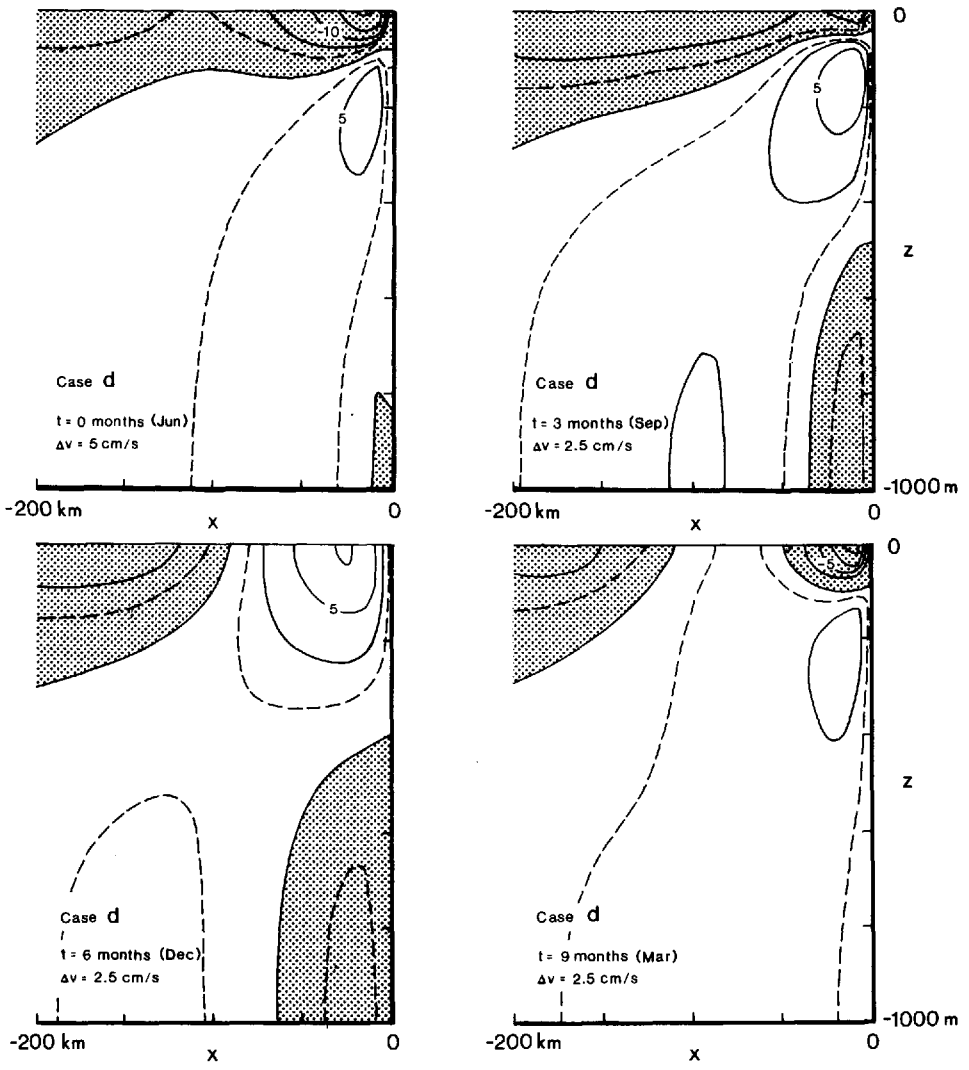

Figure 8. Zonal sections at 35N showing v for Case d in Table 1 at four times of the year when the wind is given by (11), an idealized version of the wind field off Point Conception. Dashed contours at $\pm\Delta v/2$, and regions of negative flow are shaded. Compare the summer and winter panels of this figure with the Case d solutions in Figures 2 and 5, respectively, and with the observations in Figure 1a.

increased to 2500 m (Case f). The solution was very similar to that in Figure 8, the only difference being that the current extended somewhat more deeply into the water column. This increase in depth scale was associated only with the part of the solution driven by τ^y_x; the part driven by τ^y was too surface trapped to feel the bottom to any appreciable extent.

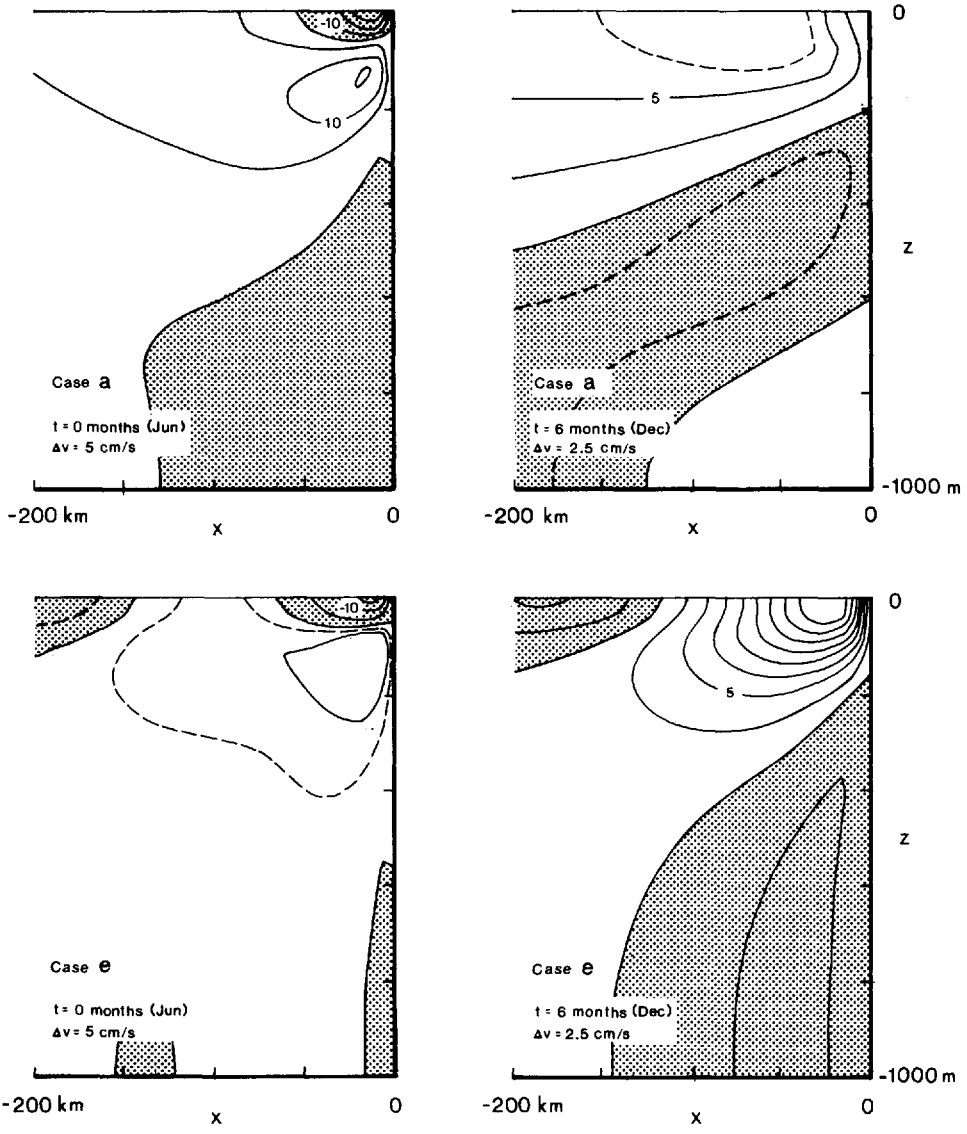

Figure 9. Zonal sections at 35N contrasting v for Cases a and e in Table 1 at two times of the year when the wind is given by (11). Dashed contours are either $\pm\Delta v/2$ or 6.25 cm/s. For Case a the resulting current system is very unrealistic, with the offshore flow always being poleward and not varying much seasonally. For Case e the flow field is more reasonable, but the poleward flow is too strong.

4. Results for the shelf model

The bottom topographic profile for the shelf model is

$$h(x) = \begin{cases} h_s, & -x_s < x \le 0 \\ h_s + \tfrac{1}{2}(H - h_s)[1 - \cos \pi(x + x_s)/s], & -s - x_s < x \le -x_s \\ H, & x \le -s - x_s, \end{cases} \quad (12)$$

where h_s is the depth of the shelf at the coast and is either 100 or 300 m, $H = 1000$ m is the depth of the ocean far offshore, and $s = 50$ km is the width of the slope. The flat portion of the shelf has a width $x_s = \Delta x$, the zonal grid step; this minimum width is required by the numerical scheme, which assumes that h_x vanishes at $x = 0$.

The background density field used is

$$\rho_b = \begin{cases} 1 + \tfrac{1}{2}\Delta\rho_1(1 - \cos \pi z/b_1) + \Delta\rho_2(1 - e^{z/b_2}), & -b_1 < z \le 0 \\ 1 + \Delta\rho_1 + \Delta\rho_2(1 - e^{z/b_2}), & -H < z \le -b_1, \end{cases} \quad (13)$$

where $\Delta\rho_1 = .0015$ gm/cm^3, $b_1 = 100$ m, $\Delta\rho_2 = .001$ gm/cm^3 and $b_2 = 500$ m. This profile is a smoother version of (10) that does not have a surface mixed layer where $N_b^2 = 0$. Such a layer cannot be included in our shelf model because the numerical scheme involves division by N_b^2 [as in Eqs. (3)].

Solutions are evaluated on a 51×31 grid in the xz-plane. The location of the offshore boundary is either at $x = -100$ or -200 km, and so the zonal grid step is either $\Delta x = 2$ or 4 km. The model employs a stretched coordinate system, with Δz varying from 33 m at $x = -L$ to 3.3 m at $x = 0$. The meridional grid step is $\Delta y = 110$ km. The values of mixing parameters are $\nu_h = 10^6$ cm^2/s and $\nu = 10$ cm^2/s, and the bottom drag coefficient is $\gamma = .001$ cm/s.

Figure 10 contrasts solutions for two different shelf depths for Case g when the wind is steady and without curl. The solutions demonstrate a tendency for the shallower shelf to strengthen the coastal jet and to weaken the undercurrent. When h_s is decreased even further to 50 m (not shown), the surface current strengthens to -42 cm/s and the undercurrent weakens to 5 cm/s. A similar, but much more severe, tendency was reported by McCreary and Chao (1985) where the shelf often acted to eliminate the undercurrent completely. The fact that the shelf has a weaker effect here is due to our use of no-slip conditions at the coast. These conditions considerably weaken the depth-averaged component of the alongshore flow over the shelf, thereby allowing the baroclinic component to be much more visible. It is also useful to contrast the deep-shelf solution in Figure 10 with the flat-bottom solution for Case d in Figure 2; the latter has somewhat weaker currents because values of ν in the flat-bottom model are greater than 10 cm^2/s away from the pycnocline.

Solutions to the shelf model were found for various parameter choices, and they corroborated all of the important conclusions from the flat-bottom solutions. For example, the coastal currents forced by τ^y are again broadened by the pycnocline and

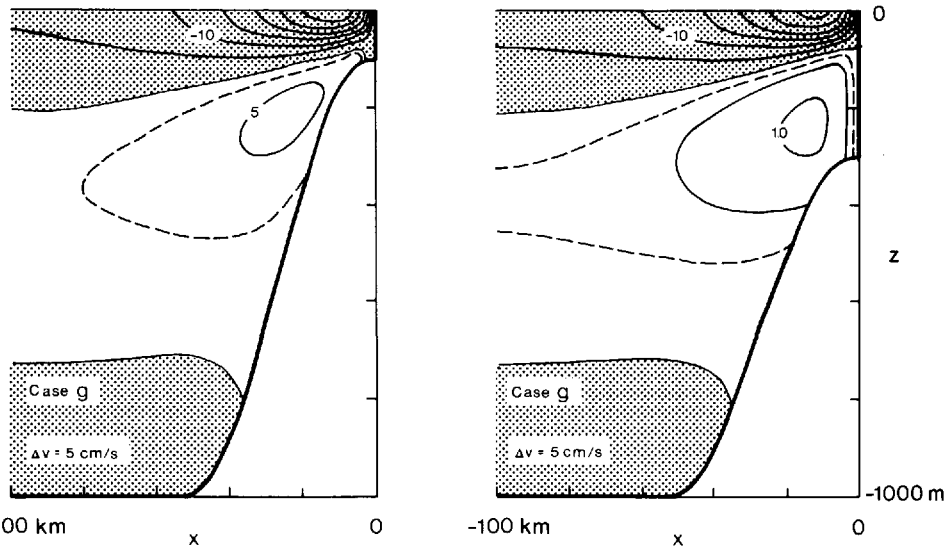

Figure 10. Zonal sections at 35N contrasting v for the different shelf depths, h_s = 100 m (left panel) and h_s = 300 m (right panel), when the wind is steady and without curl. The parameters used are those of Case g in Table 1, and $\rho_b(z)$ is given by (13). Dashed contours are $\pm\Delta v/2$, and regions of negative flow are shaded. The shelf acts to strengthen the coastal jet and to weaken the undercurrent, but not as severely as in the solutions of McCreary and Chao (1985).

strengthened by remote winds. The circulation forced by τ_x^y develops equatorward flow offshore of 100 km. The solution for Case g forced by (11) is quite similar to the flow field on a flat bottom (compare Fig. 8 with Fig. 11).

5. Dynamics

The flat-bottom model is particularly useful for discussing dynamics because solutions can be written down analytically as expansions in vertical normal modes. In this way the three-dimensional dynamics of Eqs. (1) can be understood using concepts appropriate to the two-dimensional dynamics of individual modes. We expect that many of these concepts also apply to the shelf model, since comparable solutions to the shelf and flat-bottom models are so similar.

a. The solution

Although horizontal mixing does alter the structure of solutions, it is not an essential part of the model dynamics since well-behaved solutions still exist when it is not included (McCreary, 1981). To reduce the amount of algebra required, we neglect horizontal mixing throughout the following discussion. In that case, the equations of

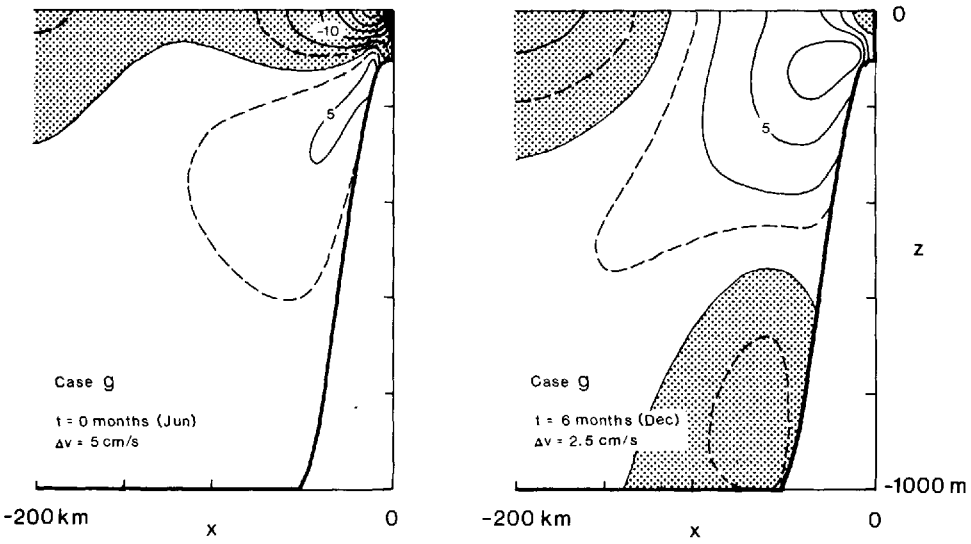

Figure 11. Zonal sections at 35N showing v for Case g in Table 1 at two times of the year when the wind is given by (11). The background density field is given by (13). Dashed contours are $\pm\Delta v/2$, and regions of negative flow are shaded. The solution is very similar to the comparable flat-bottom solution in Figure 8.

motion describing the response of the n-th vertical mode $\psi_n(z)$ are

$$p_{nxx} - \frac{\beta}{i\omega} p_{nx} - \frac{f^2}{c_n^2} p_n = -\frac{f}{i\omega} G_{nx},$$

$$v_n = \frac{p_{nx}}{f}, \tag{14}$$

$$u_n = \frac{G_n}{f} - \frac{p_{ny}}{f} + \frac{i\omega}{f^2} p_{nx},$$

where $G_n = \int_{-H}^{0} G\psi_n dz \Big/ \int_{-H}^{0} \psi_n^2 dz$ is the projection of the forcing on the mode, c_n is its characteristic speed, $\omega = \sigma + iA/c_n^2$ and $\beta = f_y$. Both vertical mixing (with $\nu = A/N_b^2$) and periodicity are included in the system through the parameter ω.

It is conceptually useful to regard solutions to (14) as being the sum of two pieces. One piece is a forced, interior response (designated below by primed variables) that exists in an unbounded ocean. The other is a coastal reaction to the interior solution (designated by double-primed variables) which is composed of free waves. The two pieces are coupled together by the boundary condition that $u_n = u_n' + u_n'' = 0$ at $x = 0$.

Let the model be forced by a wind field of limited spatial extent, that is, by a wind

patch. The solution to the first of Eqs. (14) for the interior pressure field is

$$p_n'(x, y) = \frac{f}{\omega}\frac{1}{k_1 - k_2}\left[e^{ik_1x}\int_{\infty}^{x} e^{-ik_1x'}G_{nx'}dx' - e^{ik_2x}\int_{-\infty}^{x} e^{-ik_2x'}G_{nx'}dx'\right], \quad (15)$$

where

$$k_{\binom{1}{2}} = -\frac{\beta}{2\omega}\left[1 \mp \sqrt{1 - 4\omega^2 f^2/\beta^2 c_n^2}\right], \quad (16)$$

and the other two of Eqs. (14) then give u_n' and v_n' in terms of p_n' (McCreary and Kundu, 1985). Two waves radiate away from the wind patch, the one with wavenumber $k_1(k_2)$ having either westward (eastward) group velocity or decaying to the west (east). Note that the pressure field (15) is forced only by the wind curl, and not by the wind stress itself.

The pressure field associated with the coastal reaction is a solution to the homogeneous version of (14), and is given by

$$p_n''(x, y) = e^{ik_1x}e^{-\Lambda}\int_{y_o}^{y} e^{\Lambda} f u_n'(0, y')dy', \quad (17)$$

where $\Lambda = \int^y (\omega k_1/f)dy'$, and y_o is any point equatorward of the wind patch; again, Eqs. (14) give u_n'' and v_n'' terms of p_n''. This solution is composed only of waves with the zonal wavenumber k_1. The waves with wavenumber k_2 cannot be involved, since they either have an eastward group velocity or grow exponentially offshore.

The close relationship between the interior zonal current and the coastal circulation is evident in (17). It is useful, in fact, to regard the coastal circulation as being directly forced by this interior current, rather than by the wind itself.

b. The interior response

Steady inviscid flow. The interior solution has a simple structure when the wind is steady and there is no vertical mixing, so that $\omega = 0$, $k_1 \to 0$ and $k_2 \to \infty$. The solution (15) reduces to

$$\begin{aligned} p_n' &= \frac{fG_n}{\beta}, \\ v_n' &= \frac{G_{nx}}{\beta}, \\ u_n' &= \frac{G_n}{f} - \frac{(fG_n/\beta)_y}{f} = -\left(\frac{G_n}{\beta}\right)_y, \end{aligned} \quad (18)$$

describing a baroclinic mode in a state of Sverdrup balance (McCreary, 1981). Because none of these fields involve c_n, the sum over all modes can be carried out explicitly to obtain $p' = \Sigma_{n=0}^{\infty} p_n'\psi_n = fG/\beta$, $v' = G_x/\beta$ and $u' = -(G/\beta)_y$. This

circulation is a surface-trapped flow field having the same vertical structure as the body force G. One property of this solution is that the geostrophic part of the currents, $v'_g = v' = G_x/\beta$ and $u'_g = -(fG/\beta)_y/f$, does not extend any deeper into the ocean than the Ekman drift G/f does. Another is that an equatorward flow can exist only in a region of negative wind curl.

Steady viscid flow. When there is vertical mixing and the forcing is steady, $\omega = iA/c_n^2$. Both ω and k_1 increase rapidly with modenumber, and typically only the lowest-order modes tend toward the Sverdrup balance (18). The wavenumbers of the higher-order modes satisfy the inequalities $|k_1|L_x \gg 1$ and $|k_2|L_x \gg 1$, where L_x is the zonal scale of the wind. For these modes, then, solution (15) simplifies (after two integrations by parts) to a good approximation to

$$\begin{aligned} p'_n &= \frac{c_n^2}{i\omega f} G_{nx}, \\ v'_n &= \frac{c_n^2}{i\omega f^2} G_{nxx}, \\ u'_n &= \frac{G_n}{f} - \frac{c_n^2}{i\omega f}\left(\frac{G_{nx}}{f}\right)_y, \end{aligned} \tag{19}$$

a balance that results from Ekman pumping by wind curl on the f-plane. (A third contribution to u'_n, the ageostrophic term $i\omega p'_{nx}/f$, is negligible and has been ignored.)

Because p'_n in (19) is proportional to c_n^2, its amplitude drops rapidly with n. Thus, a consequence of the shift in balance from (18) to (19) is that the high-order modes contribute much less to the total response than in the inviscid case. The effect on the total pressure field p' and the geostrophic currents is that they extend much more deeply into the water column (Fig. 5) than they do when the flow is inviscid. McCreary and Kundu (1985; see their Fig. 8) provide a relevant illustration of this type of diffusive interior flow field.

The shift in balance from (18) to (19) is also associated with a change in the zonal structure of the response of each mode. This change is illustrated in Figure 12, which shows p'_n for Case d for several modes. Because vertical mixing does not affect the barotropic mode at all, p'_o is exactly in Sverdrup balance, and has the same zonal structure as the wind, $X(x)$. As modenumber increases, damping causes a westward decay of p'_n, which eventually attains the structure X_x. (The sharp drop in p'_n at $x = 0$ for the high-order modes is eliminated by p''_n when there is a coast.) Note in Figure 12 that there are regions offshore where p'_{nx} is negative, even though the curl is positive. This property signifies that *equatorward* flow can be generated by *positive* wind curl, a direct result of vertical mixing in the model. Such a current is evident in the solution of Figures 5, 8 and 11, and is quite possibly the explanation for the observed equatorward flow offshore of 100 km in Figure 1a.

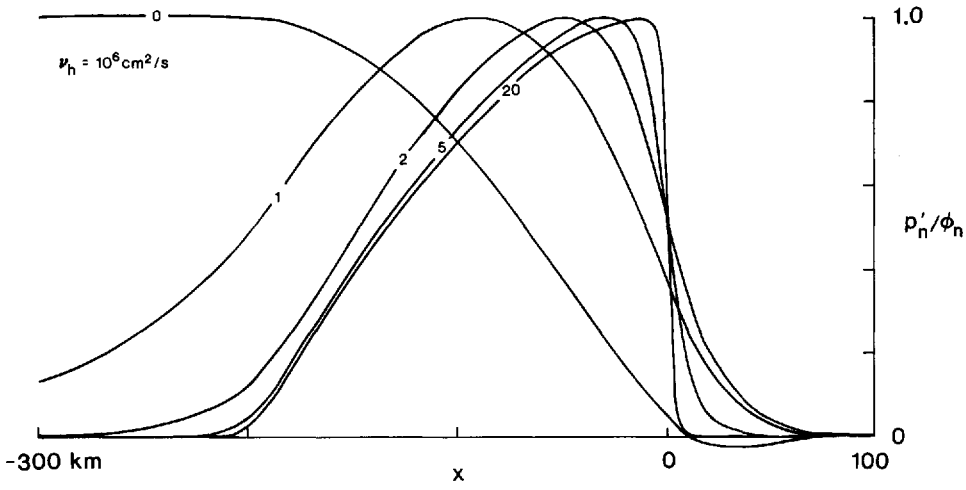

Figure 12. Zonal profiles at 35N showing p_n' for various n for Case d in Table 1 when the wind is steady. The zonal structure of the wind X is given by (6) for $x \leq 0$ and is zero for $x > 0$. The pressure fields are normalized by their minimum values ϕ_n, which are -4.5, -8.9, $-.70$, -5.5×10^{-3} and -4.2×10^{-7} cm for $n = 0$, 1, 2, 5 and 20, respectively. The values of $|\phi_n|$ drop sharply with n, indicating how weakly the higher-order modes contribute to p'. The barotropic response, p_0', has the same zonal structure as the wind, whereas p_n' for all the higher-order modes ($n \gtrsim 5$) has the structure X_x. The solution includes horizontal mixing, which acts primarily to smooth out the sharp drop in p_n' at $x = 0$. The change in structure with n is due entirely to presence of vertical mixing in the model, and allows an equatorward current to be forced by positive wind curl.

Periodic viscid flow. In this case $\omega = \sigma + iA/c_n^2$, and at the annual frequency the inequalities $|k_1|L_x \gg 1$ and $|k_2|L_x \gg 1$ hold for all the baroclinic modes (with the possible exception of the $n = 1$ mode for which $|k_1|L_x > 1$ when $L_x = 200$ km). Thus, although the barotropic mode still adjusts to the Sverdrup balance (18), all the baroclinic modes satisfy the f-plane balance (19). The offshore relative maximum of $|v|$ for Case d in Figure 7 is an interior flow of this type, with v_1' being the dominant component of v there.

c. *The coastal response*

Zonal structure. The zonal structure of the coastal response (17) is contained in the factor $\exp(-ik_1x)$. According to (16) with $\beta = 0$, k_1 is imaginary and the coastal solution decays offshore with the e-folding scale $|k_1|^{-1} = c_n/f$, the Rossby radius for all modes. With $\beta \neq 0$, however, the decay scale can be much larger than c_n/f for the low-order modes. This change in scale is illustrated in Figure 13, which shows p_n'' forced by a steady curl-free wind for Case d, both with and without horizontal mixing. It is evident in the left panel ($\nu_h = 0$) that the structure of p_n'' for the low-order modes extends farther offshore than c_n/f, whereas that for the high-order modes tends toward

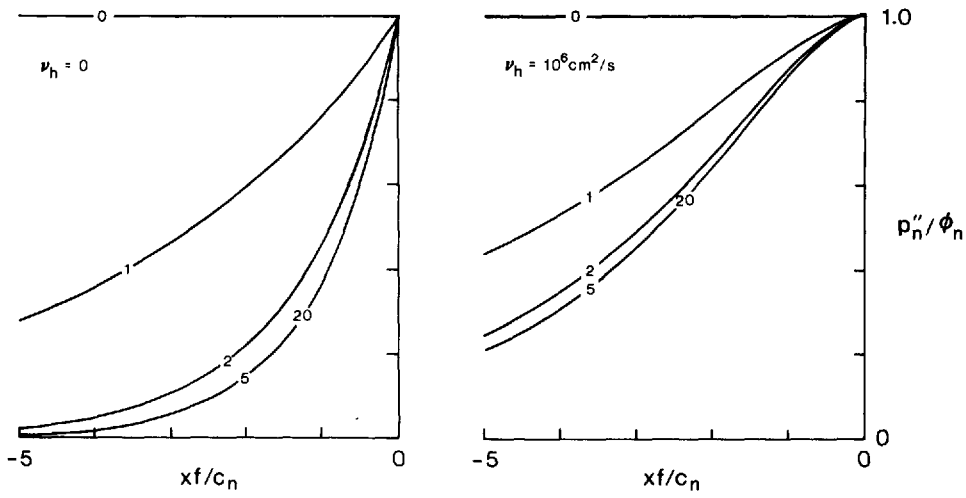

Figure 13. Zonal profiles at 35N showing p_n'' for various n for Case d in Table 1 with $\nu_h = 0$ (left panel) and with $\nu_h = 10^6$ cm^2/s (right panel) when the wind is steady and without curl. The pressure fields are normalized by their minimum values ϕ_n, which are -1.5, -11.3, -6.6, $-.24$, and -7.1×10^{-5} cm in the left panel, and 1.5, 10.5, 3.8, .068 and 2.1×10^{-5} cm in the right panel, for $n = 0$, 1, 2, 5 and 20, respectively. The horizontal axis is scaled by the Rossby radius of each mode, c_n/f, which is 1200, 15, 8, 3.2 and .76 km for $n = 0$, 1, 2, 5 and 20, respectively. Due to the β-effect, p_n'' for the low-order modes extends much farther offshore than the Rossby radius, whereas p_n'' for all the high-order modes ($n \gtrsim 5$) approaches the offshore structure that exists on the f-plane. The profiles for $n = 5$ and 20 are indistinguishable in both panels.

the profile $\exp(xf/c_n)$. The right panel ($\nu_h = 10^6$ cm^2/s) illustrates how horizontal mixing spreads p_n'' farther offshore. Note also that p_n'' for the high-order modes again tends toward a profile that is independent of n when x is scaled by c_n/f.

How far offshore the coastal flow field extends clearly depends on which modes contribute most strongly to the total solution. One factor that influences their relative contribution is the background density profile. If ρ_b is linear, then the coupling coefficient of the forcing to each mode, G_n, decreases slowly with n, and a large number of modes contribute to the total response. If ρ_b has a strong, near-surface pycnocline, G_n decreases rapidly with n, and only the lowest-order modes contribute. The coastal currents in the latter case will therefore extend farther offshore than those in the former, as can be seen in the various panels in Figure 2. (Offshore spreading due to β was not apparent in the calculations reported in McCreary, 1981, because he used a ρ_b with a weak pycnocline.)

Meridional structure. The meridional structure of the coastal response (17) is contained in the factor $e^{-\Lambda} \int_{y_o}^{y} e^{\Lambda}\, u_n'(0, y')\, dy'$. When the flow is forced only by τ^y, the interior zonal flow $u_n'(0, y)$ is Ekman flow G_n/f, which is spread throughout the forcing

region. Consequently, the integral in (17), and the associated coastal currents, increase throughout the region of the forcing (Fig. 4). In contrast, when the flow is forced only by τ^y_x, $u'_n(0, y)$ is entirely geostrophic. According to (18) and (19), $u'_n(0, y)$ is then concentrated near the northern and southern edges of the wind patch where the meridional gradients of τ^y are large, and so the coastal currents do not increase throughout the forcing region.

For example, although much of the flow in Figure 6 is associated with the interior solution v', part of it is a coastal response v'' forced by interior geostrophic currents $u'(0, y)$ that are eastward near the southern edge of the forcing (20–22.5N) and westward near the northern edge (37.5–40N). Consequently, a poleward coastal current is generated near the southern edge of the forcing and an equatorward current is generated near the northern edge, both of which decrease slowly to the north due to damping; the two currents do not cancel north of 40N, resulting in a net equatorward current which extends north of the forcing region.

Boundary waves. The type of boundary waves that contribute to (17) is determined by the zonal wavenumber k_1. With no vertical mixing in the model, the radicand in (16) vanishes at the critical latitude

$$\theta_{cr} = \tan^{-1}\left(\frac{c_n}{2R\sigma}\right), \tag{20}$$

and the nature of the waves depends on whether θ is greater or less than θ_{cr}. Equatorward of θ_{cr}, k_1 is real and the waves are offshore-propagating Rossby waves. Poleward of θ_{cr}, k_1 is complex and they are β-plane Kelvin waves that decay offshore rapidly with an e-folding scale of the order of c_n/f (Moore, 1968; McCreary, 1980).

When there is vertical mixing ω is complex, and there is no clear definition of a critical latitude. Provided that mixing is weak (as it is for the low-order modes), however, the viscid waves still have properties similar to their inviscid counterparts. In that case, the primary effect of mixing is to damp the waves in the direction of their group velocity. When mixing is strong (as it is for the high-order modes), it no longer makes sense to differentiate between Rossby and Kelvin waves.

For annual periodicity and the linear density field (9), the critical latitudes for the first three baroclinic modes are 38.2N, 32.5N and 14.7N, respectively; at 35N, then, the only possible Rossby wave occurs for the $n = 1$ mode, and the others are all β-plane Kelvin waves. Similarly, for the exponential density field (10) the critical latitudes for the first three modes are 26.1N, 14.7N and 9.9N, and *all* the boundary waves at 35N are β-plane Kelvin waves. The β-plane Kelvin waves can superpose to form a *vertically,* as well as poleward, propagating signal, just as f-plane Kelvin waves do (Romea and Allen, 1983; McCreary *et al.*, 1986).

Quasi-steadiness. A flow is quasi-steady if the effects of σ are negligible. For a

particular mode, whether the response appears quasi-steady is determined by the parameter $\omega = \sigma + iA/c_n^2$, with the response being quasi-steady if $A/c_n^2 \gg \sigma$. For the density profile (10) and with $\nu = 10$ cm^2/s, this criterion is satisfied for the $n \geq 4$ modes. Solutions forced by τ^y are therefore nearly quasi-steady (Figs. 3 and 4), because higher-order modes contribute significantly to them. In contrast the solutions forced by τ_x^y are not at all quasi-steady (Fig. 7), because they are dominated by contributions from the lowest-order modes.

Phase relations. There are interesting phase relations between the coastal currents and the forcing in Figures 3 and 7. Here we discuss the dynamical reasons for the lead of v over τ^y in Figure 3. (A similar, but somewhat more involved, explanation can be given to understand the lag of v behind τ_x^y near the coast in Figure 7.)

For τ^y forcing, $u_n'(0, y) = G_n/f$ and (17) gives

$$v_n''(x, y) = \frac{ik_1}{f} e^{ik_1 x} e^{-\Lambda} \int_{y_o}^{y} e^{\Lambda} G_n(0, y') dy'. \tag{21}$$

For the high-order modes, the response is quasi-steady and $v_n''(0, y)$ is in-phase with τ^y. For the $n = 1$ mode, $A/c_1^2 \ll \sigma$, and ω is very nearly a real number. In addition, $\theta < \theta_{cr}$ for the $n = 1$ mode at 35N for the density profile (10), and so k_1 and Λ are also real. With ω, k_1 and Λ all being real, (21) implies that $v_1''(0, y)$ *leads* τ^y by 3 months. As modenumber increases this lead decreases smoothly to zero, the quasi-steady limit. The lead is due entirely to the β-effect; with $\beta = 0$, both k_1 and Λ are imaginary, and it can be shown that $v_n''(0, y)$ *lags* τ^y for the low-order modes.

How much the total flow field $v''(0, y)$ leads τ^y depends on which modes contribute to the solution. The lead is only a few weeks for the solutions in Figure 3, because the higher-order modes contribute strongly to the flow.

6. Summary and discussion

The wind-driven circulation along an eastern ocean boundary is studied using flat-bottom and shelf models, both of which are linear, viscid and continuously stratified. One objective of this research is to investigate various mechanisms by which an equatorward wind can drive a poleward coastal current, like the Davidson Current. Another, and equally important, objective is to understand how equatorward flow is forced in a region of positive wind curl, like that off California.

Solutions forced by a steady, equatorward wind without curl τ^y develop an equatorward coastal jet and a poleward undercurrent (Fig. 2). Due to β and ν_h the width of these currents is not necessarily limited by the Rossby radii of the contributing modes (Fig. 13), with the β-broadening being most effective when ρ_b has a pycnocline. The speed of the coastal currents depends on the meridional structure of the wind, increasing when the forcing includes remote winds located to the south. If τ^y oscillates

at the annual cycle, solutions are similar in structure to their steady counterparts, indicating that part of the response is quasi-steady in character. Phase propagates upward, offshore and poleward, indicating that another part consists of propagating waves, either Rossby waves or β-plane Kelvin waves (Figs. 3 and 4). The maximum surface current leads the wind by several weeks, a property that is due to the β-effect.

For all of the solutions driven by a curl-free wind, the surface current flows everywhere in the direction of the wind (except for the periodic solution for a brief time when the wind changes direction). The solutions therefore suggest that remote forcing cannot account for the appearance of the Davidson Current, since the winter winds off Baja California are never directed poleward. The relaxation of the wind associated with the annually varying wind field $\tau^y = \tau_o\, Y(y)\, (.5 + .4e^{-i\sigma t})$ does cause a poleward surface current. This current, however, is shallower and weaker than the observed Davidson Current, suggesting that the wintertime relaxation of the wind off California is not the primary cause of the Davidson Current.

Solutions forced by a steady, positive wind curl τ^y_x (with $\tau^y = 0$ at $x = 0$) develop a deep, broad, poleward current near the coast and an equatorward current farther offshore (Figs. 5 and 6). The equatorward current exists in a region of positive curl, and owes its existence to the presence of vertical mixing in the model (Fig. 12). In contrast to the solutions forced by τ^y, solutions are not very dependent on parameters, because much of the flow is an interior current that is directly forced by the wind curl; in particular, current speeds do not increase when remote winds are included. Solutions forced by an annually periodic wind curl are not at all quasi-steady, since they are dominated by contributions from the lowest-order modes (Fig. 7).

Solutions driven by the wind field (11), an idealized representation of the forcing off California, compare favorably with observations, but only when $\rho_b(z)$ has a realistically sharp, near-surface pycnocline and the remote winds off Baja California are included in the forcing (Figs. 8 and 9). This success suggests the following conclusions. Positive wind curl generates both the poleward Davidson Current and the equatorward flow offshore of 100 km. Equatorward winds drive a coastal jet that is spread offshore by the pycnocline and strengthened by the remote winds. During the summer, this jet is sufficiently strong to overwhelm the poleward flow due to the wind curl.

The presence of a shelf strengthens the coastal surface jet and weakens the undercurrent, but does not significantly affect the currents farther offshore (Fig. 10). The weakening of the undercurrent was much more severe in the shelf solutions reported by McCreary and Chao (1985), due to their use of a slip condition at the coast. The shelf solutions are all similar to corresponding flat-bottom solutions, including those that simulate the California Current system (Fig. 11).

The models studied here are dynamically too simple to be able to explain all properties of the flow off California. For example, since ρ is fixed at the ocean surface, the models cannot generate any sea-surface-temperature variability. In addition, the lack of nonlinearities prevents the surface currents from ever going unstable, whereas

the presence of eddies is a ubiquitous feature of the observed flow. Nevertheless, the models are able to simulate major features of the circulation, suggesting that they contain much of the fundamental dynamics involved in the California Current system. In particular, they indicate the dynamical importance of vertical and horizontal mixing, the near-surface pycnocline, and the remote winds off Baja California. We expect that these factors will also be important in dynamically more sophisticated models of the region.

Acknowledgments. This work was supported by ONR Grant No. N00014-85-K-0019 and by NSF Grant No. OCE-85-09752. Some of the computations using the shelf model were performed on the CRAY-1 computer at the National Center for Atmospheric Research; NCAR is supported by the National Science Foundation. Ken Brink's comments on an earlier version of this paper are much appreciated. We also thank Kevin Kohler for his programming assistance and Kathy Maxson for drafting the figures.

REFERENCES

Chelton, D. B. 1984. Seasonal variability of alongshore geostrophic velocity off central California. J. Geophys. Res., *89,* 3473–3486.

Godfrey, J. S. and K. R. Ridgway. 1985. The large scale environment of the poleward flowing Leeuwin Current, western Australia: Longshore steric height gradients, wind stresses and geostrophic flow. J. Phys. Oceanogr., *15,* 481–495.

Hickey, B. M. 1979. The California current system—hypothesis and facts. Prog. Oceanogr., *8,* 191–279.

Lynn, R. J., K. A. Bliss and L. E. Eker. 1982. Vertical and horizontal distributions of seasonal mean temperature, salinity, sigma-*t*, stability, dynamic height, oxygen, and oxygen saturation in the California Current, 1950–1958. California Cooperative Oceanic Fisheries Investigations Atlas No. 30, La Jolla, CA 613 pp.

McCreary, J. P. 1980. Modelling wind-driven ocean circulation. Tech. Rept. HIG-80-3, Hawaii Inst. Geophys., Honolulu, HI, 64 pp.

—— 1981. A linear stratified ocean model of the coastal undercurrent. Phil. Trans. Roy. Soc., London, A *302,* 385–413.

McCreary, J. P. and S.-Y. Chao. 1985. Three-dimensional shelf circulation along an eastern ocean boundary. J. Mar. Res., *43,* 13–36.

McCreary, J. P. and P. K. Kundu. 1985. Western boundary circulation driven by an alongshore wind: with application to the Somali Current system. J. Mar. Res., *43,* 493–516.

McCreary, J. P., S. R. Shetye and P. K. Kundu. 1986. Thermohaline forcing of eastern boundary currents: with application to the circulation off the west coast of Australia. J. Mar. Res., *44,* 71–92.

Moore, D. W. 1968. Planetary-gravity waves in an equatorial ocean. Ph.D. thesis, Harvard University, Cambridge, MA.

Munk, W. H. 1950. On the wind-driven ocean circulation. J. Meteor., *7,* 79–93.

Nelson, C. S. 1977. Wind stress and wind stress curl over the California Current. Tech. Rept. NMFS-SSRF-714, Natl. Oceanic and Atmos. Admin., Washington, D.C.

Philander, S. G. H. and P. Delecluse. 1983. Coastal currents in low latitudes (with application to the Somali and El Niño currents). Deep-Sea Res., *30,* 887–902.

Philander, S. G. H. and J.-H. Yoon. 1982. Eastern boundary currents and coastal upwelling. J. Phys. Oceanogr., *12,* 862–879.

Romea, R. D. and J. S. Allen. 1983. On vertically propagating coastal Kelvin waves at low latitudes. J. Phys. Oceanogr., *13,* 1241–1254.

Sverdrup, H. U., M. W. Johnson and R. H. Fleming. 1942. The Oceans: Their Physics, Chemistry and General Biology. Prentice-Hall, Inglewood Cliffs, NJ, 108 pp.

Received: *4 June, 1986;* revised: *24 October, 1986.*